

Exploiting billiard theory to calculate the mean path length of light in refractive spheroidsMatt Majic^{*,} Walter Somerville,[†] and Eric C. Le Ru[‡]*The MacDiarmid Institute for Advanced Materials and Nanotechnology, School of Chemical and Physical Sciences, Victoria University of Wellington, PO Box 600 Wellington, New Zealand* (Received 15 May 2022; accepted 14 July 2022; published 25 July 2022)

A technique is introduced to calculate the mean path length of light rays diffusely incident on a refractive object. It uses the phase portrait from billiard theory to determine the criteria for which chords are accessible for a given refractive index. The mean path length is given as an integral over the lengths of chords accessible via refraction, which implicitly accounts for total internal reflections. We demonstrate this method by calculating the mean path length in ellipses and spheroids. The mean path length is given by a double integral for the ellipse and a triple integral for the spheroid, which may be evaluated numerically, and also allows us to deduce simple series expansions for low eccentricity. These results give analytic expressions for the orientation averaged absorption cross sections in the geometric optics limit.

DOI: [10.1103/PhysRevA.106.013521](https://doi.org/10.1103/PhysRevA.106.013521)**I. INTRODUCTION**

This study aims to calculate the mean path length traveled by light rays diffusely incident on a refractive spheroid in the geometric optics limit. The purpose of calculating the mean path length is that it applies as the short wavelength limit to the electromagnetic scattering problem for a wave incident on a dielectric boundary, in particular the mean path length is directly related to the absorption of a weak absorber. This is a followup on two recent papers [1,2], which studied the mean path length in simple geometries such as spheres, cubes, cylinders, polygons, and prisms. Those geometries were treated with ideas that only apply in specific circumstances with high symmetry, while this paper aims to make a step in the direction of more complex analytical calculations with ellipses and spheroids, introducing techniques from billiard theory that should allow generalization to more complex shapes. Spheroids are a common model for atmospheric aerosols and in solution [3], where analytic solutions are known in terms of the T-matrix method. However, computations are difficult for large particles, and no large size asymptotic expressions are known for the absorption in the weakly absorbing case. The mean path length derived here will provide an expression for the high-frequency limit of the absorption cross section.

We may now note some simple theorems for general shapes. For nonrefractive convex bodies one can simply use the mean chord length theorem [4–7], which states that the mean chord length $\langle C \rangle$ depends only on the ratio of volume V to surface area Σ as $\langle C \rangle = 4V/\Sigma$. For nonrefractive bodies with imperfections that scatter the light into a random walk, the similar mean path length theorem applies. This states that

the mean path length traveled by the rays inside the object is still $\langle L \rangle = 4V/\Sigma$, independent of the scattering properties [8].

For refractive objects with scattering, the problem is also simple and given by

$$\langle L_{\text{sca}} \rangle = 4 \frac{V}{\Sigma} s^2 \quad (1)$$

for refractive index s relative to its surroundings [9]. This surprisingly is independent of the amount of scattering, as long as it is nonzero.

But for perfectly nonscattering refractive objects, the mean path length is much more complex due to refraction and internal reflections. There is no overarching theorem for calculating the mean path length and so far only simple geometries such as spheres and regular polygons have been studied analytically [1,2,10]. Billiard theory is a well-studied area of mathematics, which analyzes the different types of trajectories of billiard balls confined to a billiard table of any shape. The balls can be interpreted as light rays, which reflect off a boundary in the same way, if one then also adds the refractive effects. This link has been explored in the past two decades in relation to whispering gallery modes in hexagonal optical cavities [11,12], deformed circular cavities [13–15], quasibound modes in partially chaotic refracting billiards [16], and the escape of trapped modes [17,18].

While zero scattering of any kind is unachievable, the nonscattering case determines the limit of the absorption of a weakly absorbing object when scattering is weaker than absorption [1]. This is therefore relevant to applications to particles such as aerosols, where the absorption together with the extinction (of twice the particle area) are important optical properties [19–21]. This study focuses purely on the geometric optics limit, while wave effects such as dispersion and interference may be added to increase the range of validity to smaller particles [22–29].

In this paper we consider the zero-scattering case of ellipses and spheroids, and devise a method of calculating the

*mattmajic@gmail.com

†waltersom@gmail.com

‡eric.leru@vuw.ac.nz

mean path length via concepts in billiard theory. The results are expressed as integrals, which are tested against Monte Carlo simulations. We then consider the general implications of billiard theory on the mean path length through particles of arbitrary shape.

II. ELLIPSE

We will study the ellipse first to introduce the general method before applying it to spheroids.

A. No refraction

First let us consider just the average chord length with $s = 1$, meaning no refractive boundary. An ellipse lies in the xz plane with width $2a$ along x and $2c$ along z , in a diffuse distribution of rays, which may cross the ellipse, tracing out chords. The mean chord length $\langle C_{2D} \rangle$ could be calculated simply by using the two-dimensional (2D) mean path length theorem (Cauchy's formula),

$$\langle C_{2D} \rangle = \pi \frac{A}{P} \quad (2)$$

with area $A = \pi ac$ and perimeter $P = 4cE_i(e^{-2})$, where E_i is the complete elliptic integral of the second kind and $e = \sqrt{1 - a^2/c^2}$ is the eccentricity.

$$C(\theta, z) = \frac{2a(a^2z^2 - c^2z^2 + c^4)^{3/2}}{2acz(a^2 - c^2)\sqrt{c^2 - z^2} \sin \theta + (a^4z^2 - a^2c^4 - c^4z^2 + c^6) \cos \theta + a^2c^4 \sec \theta}. \quad (6)$$

The integral (5) agrees numerically with Cauchy's formula (2).

B. Refraction

For a refractive boundary, when a ray hits the surface with angle θ_i it has a probability of reflecting back out, or refracting in to an angle θ to the normal according to Snell's law:

$$\sin \theta = \frac{1}{s} \sin \theta_i \quad (7)$$

while the ray cannot refract in to an angle θ greater than the critical angle θ_c where

$$\theta_c = \text{asin} \frac{1}{s}. \quad (8)$$

All incident rays that refract through the boundary get compressed into the range $|\theta| \leq \theta_c$, and rays inside the ellipse that hit the boundary at an angle θ' to the normal will undergo total internal reflection if $|\theta'| > \theta_c$. Once inside it may reflect back inside any number of times before finally refracting out. An example of a ray reflecting once inside an ellipse is shown in Fig. 1. Probabilistic reflections are also possible, with probabilities given by the Fresnel coefficients, but to simplify the problem we may replace all probabilistic reflections with refractions since this does not affect the mean path length, as proved in Ref. [1] and supported by Monte Carlo simulations.

We define the path length of a ray as the total distance traveled by the ray inside the object. Naively the mean path length

But for purposes of generalizing to refractive ellipses, we will calculate the mean path length as an integral over the phase space. The chord length C depends on the point of incidence x, z and the entry angle θ to the normal. The rays are incident on the perimeter in a uniform distribution $1/P$ with respect to arc length t , and at each point, rays are distributed about θ in a Lambertian distribution with probability density $\frac{1}{2} \cos \theta$. For any 2D shape, the mean chord length is given the following integral over all chords:

$$\langle C_{2D} \rangle = \frac{1}{P} \int_0^P \int_{-\pi/2}^{\pi/2} C(\theta, t) \frac{1}{2} \cos \theta d\theta dt. \quad (3)$$

For an ellipse we must parametrize in terms of z because there is no straightforward analytic expression for the chord length C directly in terms of t . For an ellipse, the infinitesimal arc length dt is related to dz by

$$dt = \frac{dt}{dz} dz = \sqrt{1 + \left(\frac{dx}{dz}\right)^2} dz = \sqrt{1 + \frac{a^2z^2}{c^2(c^2 - z^2)}} dz \quad (4)$$

so the mean chord length may be expressed as

$$\langle C_{\text{ellipse}} \rangle = \frac{2}{P} \int_0^c \int_{-\pi/2}^{\pi/2} C(\theta, z) \cos \theta \frac{dt}{dz} d\theta dz, \quad (5)$$

where $C(\theta, z)$ is calculated in Appendix A as

can be calculated by generalizing the integral (3); replacing the chord length C with path length L , changing the bounds of integration for θ by $\pm\theta_c$ and renormalizing the Lambertian distribution to $\frac{s}{2} \cos \theta$ [1]:

$$\langle L_{2D} \rangle = \frac{1}{P} \int_{-\theta_c}^{\theta_c} \int_0^P L(\theta, t) dt \frac{s}{2} \cos \theta d\theta, \quad (9)$$

but calculating $L(\theta, t)$ would be extremely complex, as one would have to determine if and how many times the ray will undergo total internal reflection, and how long each of the chord lengths are.

Instead, the main idea in this work is to calculate the mean path length by integrating over all free chords: the chords that are accessible by rays that refract in from outside. For this we use the concept of a phase space from billiard theory.

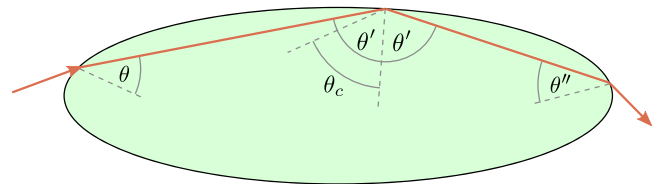


FIG. 1. Light ray refracting through an ellipse, refracting in at an angle $\theta < \theta_c$, reflecting inside at an angle $\theta' > \theta_c$ to the normal, and refracting out from an angle $\theta'' < \theta_c$.

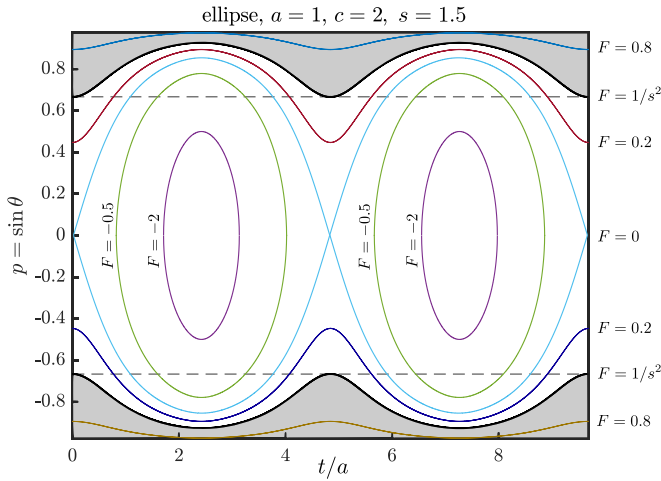


FIG. 2. Phase portrait for an ellipse of aspect ratio 2, refractive index $s = 1.5$, showing a range of curves for $F = -2, -0.5, 0, 0.2, 1/s^2 \approx 0.444, 0.8$. $F = -2$ are the innermost purple ovals, which are part of the same orbit that crosses the focal line. $F = 0$ is called the separatrix where rays pass through the foci. $F = 0.8$ defines clockwise and anticlockwise whispering gallery modes. The black dashes mark $p = \pm 1/s$ where rays leave the billiard if they pass below this line. $F = 1/s^2$ (black) mark the innermost curves that lie entirely in the range $|p| \geq 1/s$, and divide the free region (white) and trapped regions (gray) of the phase space.

C. Elliptical billiard and its phase portrait

A billiard is basically an idealized billiard table where point billiard balls are fired in straight lines and reflect inwards off the boundary. This is similar to our refracting object, but in our case the light enters in from outside and may also leave, hence refracting objects are sometimes called “open billiards” [30], and we may use the term “closed billiard” for the other type. Trajectories, also known as orbits, are described on a phase space, which encodes the points and angles on the boundary. Specifically, the phase space is a two-dimensional space parameterized by arc length $t \in [0, P)$ around the perimeter, and angle $\theta \in [-\pi/2, \pi/2]$ to the normal inside the surface. Each time a ray hits the boundary it puts a mark on the phase space according to its point and angle of incidence. An orbit in a closed billiard maps out infinitely many points as the ray is trapped. An example of a phase space with a few select orbits is shown in Fig. 2.

For an open billiard we can divide the phase space into two regions corresponding to free and trapped modes. The free regions of the phase space are those that can be reached by rays incident from outside, and the rest of the phase space is trapped. We know at least all points on the phase space with $|\theta| < \theta_c$ are free due to direct refraction from outside, but the free phase space also includes points and angles that a ray can reach via total internal reflection.

If no scattering is present, the trapped phase space is unoccupied while the free phase space is uniformly filled with a density of s (or s^2 in three dimensions) relative to outside. For all points with $|\theta| < \theta_c$, the factor of s is due to the compression of angles as the light refracts in. The rest of the free phase space must also have a density of s , which can be

justified by considering that the rates of flux in and out of this region must be equal to maintain equilibrium.

If any amount of scattering is present, the entire phase space is free and uniformly filled with a density of s . This is backed by Monte Carlo simulations, and an argument for this is presented in Ref. [2], which applies to arbitrarily low scattering.

A key observation is that the mean path length is proportional to the total ray mass inside the object. This mass is the integral of the ray density over the phase space, weighted by the chord lengths corresponding to each point. In the scattering case the mean path length is the integral over all chord lengths in the phase space filled with a uniform density of s (or s^2 in three dimensions), which evaluates to $s\pi A/P$ (or $s^2 4V/\Sigma$ in three dimensions). Similarly in the nonscattering case the mean path length is the integral of the chord lengths, but only over the free (populated) regions of the phase space.

So we need to determine exactly where the boundary between the free and trapped subspaces lies. For very simple objects where every point on the perimeter is identical—circles, spheres, infinite strips, slabs, and cylinders, no total internal reflection can occur so the boundary is simply $\theta = \theta_c$. For polygons the boundary is also independent of t [2].

Ellipses and ellipsoids are also special cases, because their phase spaces are nonergodic, which means that any thin beam of rays will follow a predictable curve in the phase space. For the ellipse these curves are parameterized by Refs. [31,32], denoting $p = \sin \theta$:

$$p(t, F) = \pm \sqrt{F - \frac{e^2(F-1)}{(1-e^2)^2 z^2/x^2 + 1}}, \quad (10)$$

where $e = \sqrt{1 - a^2/c^2}$ is the eccentricity and we have used z and x in place of arc length t , because the expression in terms of t is not easily expressed analytically. F is a constant of motion, which defines the orbit uniquely up to a reverse of its direction. Physically F is related to the product of the angular momenta of the ball about the two foci of the ellipse [31], and ranges from $-1/(1 - e^{-2})$ (oscillation across the narrow part of the ellipse on the x axis) to 1 (grazing clockwise or anticlockwise around the perimeter). The phase space of an ellipse is shown in Fig. 2 with contours of Eq. (10) for selected values of F . The portrait shows two types of curves: waves and double ovals. In a closed billiard, the waves correspond to rays traveling around the ellipse in one direction, anticlockwise for $p > 0$ and clockwise for $p < 0$. The ovals come in pairs for t and $t + P/2$ corresponding to the same orbit, where the ball bounces across the thinner width of the ellipse, avoiding the tips.

Now considering the open billiard, rays are still confined to the same curves, but only curves that extend into the region $|p| < 1/s$ ($|\theta| < \theta_c$) may be populated by rays refracting in from outside the billiard. Any curve of the double-oval type ($F < 0$) is free since these loops touch $p = 0$, while only some wave-type trajectories are free. All free trajectories lie between the two wavelike curves that touch $p = \pm 1/s$ at their minimum value of $|p|$, which occurs at the tips $t = 0, P/2$. These curves are parameterized by $F = 1/s^2$, and we denote

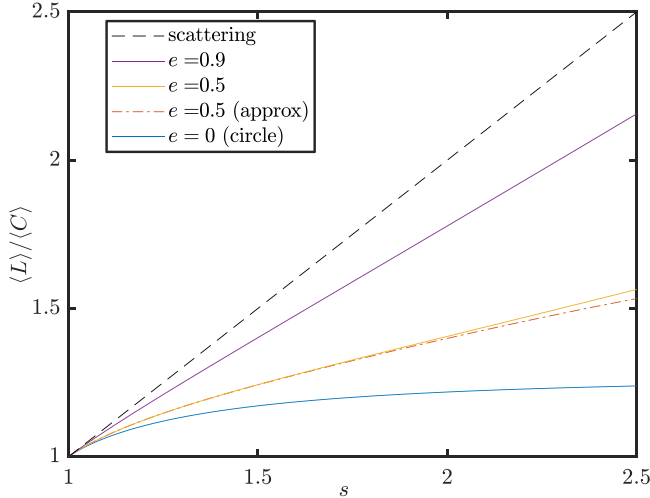


FIG. 3. Mean path length in an ellipse for a range of refractive indices s and eccentricities e , as calculated by the integral (12), normalized by the mean chord length. The dashed line is the mean path length when scattering is included.

them by p_f (f for free):

$$p_f = p \left(z, F = \frac{1}{s^2} \right) = \frac{1}{s} \sqrt{1 + \frac{e^2(s^2 - 1)}{(1 - e^2)^2 z^2 / x^2 + 1}} \quad (11)$$

and an example is plotted in black in Fig. 2, enclosing the white region, which is the free phase space.

D. Mean path length

Now we can calculate the mean path length under diffuse illumination. This is calculated by integrating the chord length $C(\theta, t)$, given in Eq. (6), over the free phase space $|p| < p_f$, times the ray density, which we argued in Sec. II C is uniformly equal to s . We parametrize this in terms of p, z as

$$\langle L_{\text{ellipse}} \rangle = \frac{s}{P} \int_{-p_f}^{p_f} \int_{-c}^c C(p, z) \frac{dt}{dz} dz dp. \quad (12)$$

This is evaluated numerically and plotted in Fig. 3 for a range of aspect ratios and refractive indices. Monte Carlo simulations of 10^8 rays were also used to calculate the mean path length (which included the Fresnel probabilities). The integral (12) agrees with Monte Carlo simulation data to within a relative error of $\sim 10^{-5}$, about the standard deviation of the simulation.

The integral can also provide simple approximations in the limit as the aspect ratio e goes to zero, i.e., as the ellipse tends towards a circle. Expanding $P, dt/dz, C, p_f$ and keeping only terms up to order e^4 gives for the mean path length:

$$\begin{aligned} \frac{\langle L_{\text{ell}} \rangle}{\langle C_{\text{ell}} \rangle} &= \frac{2}{\pi} \left(s\theta_c + \sqrt{1 - \frac{1}{s^2}} \right) + \frac{(s^2 - 1)^{3/2}}{\pi s} e^2 \\ &+ (4 - 3s^2) \frac{(s^2 - 1)^{3/2}}{16\pi s} e^4 + O(e^6). \end{aligned} \quad (13)$$

This is plotted alongside the exact integral in Fig. 3, which shows it is a good approximation for $e \lesssim 0.5$ ($c/a \lesssim 1.15$) in

the range $s \leq 2$ (accuracy decreases with s). For $e = 0.5$, the fourth-order term is only beneficial for $s \lesssim 3$.

In the limit of high eccentricity, $e \rightarrow 1$, the trapped region of the phase space shrinks and the mean path length tends towards that in the scattering case, Eq. (1). Correction terms in the expansion are difficult to determine due to singularities in the integrand.

III. PROLATE SPHEROID

The mean path length in a spheroid can be calculated using the same technique of integrating the chord length over the phase space of free orbits. We use spheroidal coordinates (ξ, η, ϕ) , with focal length $2f$:

$$\xi = \frac{\sqrt{(z+f)^2 + \rho^2} + \sqrt{(z-f)^2 + \rho^2}}{2f} \quad (14)$$

$$\eta = \frac{\sqrt{(z+f)^2 + \rho^2} - \sqrt{(z-f)^2 + \rho^2}}{2f}, \quad (15)$$

where $\rho^2 = x^2 + y^2$. $\xi \in [1, \infty)$ defines a spheroidal surface with semimajor axis c along z and semiminor axis a , while $\eta \in [-1, 1]$ is analogous to the latitude, and ϕ is the usual azimuthal angle.

A. Constants of motion

The constants of motion of a given ray's orbit (in a closed billiard) are important to us because they define curves and surfaces (in three dimensions) on the phase space, for which we want to compare to the critical angle and the boundary between free and trapped modes. The phase spaces of spheroids have been analyzed in Ref. [33,34] using Hamiltonian mechanics. For clarity we will follow their derivations in detail to obtain the phase space curves and surfaces, before linking these to free and trapped modes in Sec. III B.

Consider a closed spheroidal billiard, where a ray may be taken as a unit point mass inside with fixed velocity, whose kinetic energy (the Hamiltonian) can be expressed as

$$H = \frac{1}{2} (v_\xi^2 + v_\eta^2 + v_\phi^2) \quad (16)$$

$$= \frac{f^2}{2} \left(\frac{\xi^2 - \eta^2}{\xi^2 - 1} \dot{\xi}^2 + \frac{\xi^2 - \eta^2}{1 - \eta^2} \dot{\eta}^2 + (\xi^2 - 1)(1 - \eta^2) \dot{\phi}^2 \right), \quad (17)$$

where, for example, v_ξ is the speed of the ball in direction $\hat{\xi}$, and $\dot{\xi}$ is the time derivative of ξ . The conjugate momenta P_ξ, P_η, P_ϕ are determined by Hamilton's equations:

$$P_\xi = \frac{\partial H}{\partial(f\dot{\xi})} \quad P_\eta = \frac{\partial H}{\partial(f\dot{\eta})} \quad P_\phi = \frac{\partial H}{\partial(f\dot{\phi})}. \quad (18)$$

Using conjugate momenta, the Hamiltonian is then expressed in a separable form:

$$H = \frac{1}{2} \left(\frac{\xi^2 - 1}{\xi^2 - \eta^2} P_\xi^2 + \frac{1 - \eta^2}{\xi^2 - \eta^2} P_\eta^2 + \frac{P_\phi^2}{(\xi^2 - 1)(1 - \eta^2)} \right). \quad (19)$$

One advantage of using spheroidal coordinates is that reflections in the spheroid are simply described by

$$(\xi, \eta, \phi, P_\xi, P_\eta, P_\phi) \rightarrow (\xi, \eta, \phi, -P_\xi, P_\eta, P_\phi) \quad (20)$$

so that reflections do not affect any of the terms in the Hamiltonian (19). The equations of motion are straight lines, which can be expressed in spheroidal coordinates via separation of variables. Multiplying H by $(\xi^2 - \eta^2) = (\xi^2 - 1) + (1 - \eta^2)$, it can be separated into terms containing only ξ , η , or ϕ . And conservation of energy implies $H = E$ for constant E , so Eq. (19) becomes

$$(\xi^2 - \eta^2)2E = (\xi^2 - 1)P_\xi^2 + (1 - \eta^2)P_\eta^2 + \frac{P_\phi^2}{\xi^2 - 1} + \frac{P_\phi^2}{1 - \eta^2} \quad (21)$$

and E simply scales the particle's speed so we may set $E = 1/2$.

There are two constants of motion. First, P_ϕ must be constant since it is the only ϕ -dependent term and physically is the angular momentum about the z axis. Geometrically P_ϕ is proportional to the closest approach of the ray to the z axis. For instance, a ray with $P_\phi = 0$ travels exactly as it would in an ellipse in the x - z plane. The other constant is determined by noting that the ξ - and η -dependent parts of (21) should not vary individually, so we may set them equal to constants $\pm\kappa^2$:

$$(\xi^2 - 1)P_\xi^2 + \frac{P_\phi^2}{\xi^2 - 1} - \xi^2 = -\kappa^2 \quad (22)$$

$$(1 - \eta^2)P_\eta^2 + \frac{P_\phi^2}{1 - \eta^2} + \eta^2 = \kappa^2. \quad (23)$$

Equation (23) shows that P_ϕ is maximized for $P_\eta = 0$, $\eta = 0$; here $P_\phi = \kappa$ and motion is restricted to the equator. And Eq. (22) shows that P_ϕ is further maximized for $P_\xi = 0$, giving $P_{\phi \max} = \pm\sqrt{\xi^2 - 1}$, and in this case the rays reflect off the equatorial surface at infinitesimally small intervals, essentially traveling in a circle around the equator. So the range of P_ϕ^2 is

$$0 \leq P_\phi^2 \leq \xi^2 - 1.$$

And for a fixed P_ϕ , one can determine the range of κ to be

$$P_\phi^2 \leq \kappa^2 \leq \xi^2 - \frac{P_\phi^2}{\xi^2 - 1}.$$

B. Phase space and the boundary between free and trapped modes

Having determined the constants of motion, we want to consider their corresponding curves in the phase space. The phase space for a spheroid is technically four dimensional; chords are described by two coordinates for the surface point, η , ϕ , and two angles for the ray's direction, θ , φ , where φ is the angle of rotation about the surface normal. Due to the rotational symmetry of a spheroid we can ignore the azimuthal surface coordinate ϕ , so the phase space is effectively three dimensional.

We may also now consider the open billiard, and which constants of motion correspond to free or trapped modes. A ray will undergo total internal reflection when $p \equiv \sin \theta > 1/s$ (note that in three dimensions, $0 \leq \theta \leq \pi/2$ and $0 \leq p \leq 1$). p is related to the velocities as

$$p = \frac{\sqrt{v_\eta^2 + v_\phi^2}}{\sqrt{v_\xi^2 + v_\eta^2 + v_\phi^2}}, \quad (24)$$

where the velocities can be converted into the conjugate momenta via

$$v_\xi = \sqrt{\frac{\xi^2 - 1}{\xi^2 - \eta^2}} P_\xi \quad (25)$$

$$v_\eta = \sqrt{\frac{1 - \eta^2}{\xi^2 - \eta^2}} P_\eta \quad (26)$$

$$v_\phi = \frac{P_\phi}{\sqrt{(\xi^2 - 1)(1 - \eta^2)}} \quad (27)$$

and P_ξ , P_η can in turn be expressed in terms of κ , P_ϕ , and η by solving Eqs. (22), (23), to give

$$p(\eta, \kappa, P_\phi) = \sqrt{\frac{(\kappa^2 - \eta^2)(\xi^2 - 1) + P_\phi^2}{(\xi^2 - \eta^2)(\xi^2 - 1)}}. \quad (28)$$

It will also be convenient for us to express P_ϕ and κ in terms of the angle of rotation around the surface normal φ , since the distribution of rays is uniform with respect to φ . This is related to the velocities as

$$\cos \varphi = \frac{v_\eta}{\sqrt{v_\phi^2 + v_\eta^2}}. \quad (29)$$

For $\varphi = 0, \pi$, rays cross the z axis and bounce as if they were in an ellipse, and for $\varphi = \pm\pi/2$, the rays bounce in a circle on the equator, with $p(\eta, \pm\pi/2)$ constant.

If we parametrize the phase space by $p \in [0, 1]$, $\eta \in [-1, 1]$, $\varphi \in (-\pi, \pi]$, each set of constants κ , P_ϕ defines a curve $p(\eta)$, $\varphi(\eta)$ for which any one ray must be confined to, and a curve $\kappa(P_\phi)$ defines a surface $p(\eta, \varphi)$. For a given refractive index s , there is a critical surface $p_f(\eta, \varphi)$ defined by $\kappa = \kappa_f(P_\phi)$, where the minimum value of p_f is $1/s$. All free chords lie in the phase space volume $0 \leq p \leq p_f(\eta, \varphi)$. In order to find p_f , we must find where $p(\eta, \kappa_f, P_\phi)$ is minimized in terms of η , and equate this value of p to $1/s$ to solve for $\kappa_f(P_\phi)$. Equation (28) tells us that $p(\eta, \kappa_f, P_\phi)$ is minimized at $\eta^2 = \eta_0^2 = \frac{1}{2}(\kappa^2 + 1 - \sqrt{(\kappa^2 - 1)^2 + 4P_\phi^2})$ (not all orbits reach the tips $\eta = \pm 1$). Substituting this into Eq. (28), the condition $p_f(\eta_0, \kappa_f, P_\phi) = 1/s$ tells us $\kappa_f(P_\phi)$:

$$\kappa_f^2 = 1 + \frac{\xi^2 - 1}{s^2} - \frac{P_\phi^2 s^2}{\xi^2 - 1}. \quad (30)$$

This is illustrated in the κ, P_ϕ space in Fig. 4. To obtain the corresponding surface in the phase space $p_f(\eta, \varphi)$, we want to express P_ϕ in terms of η, φ when $\kappa = \kappa_f$. This is

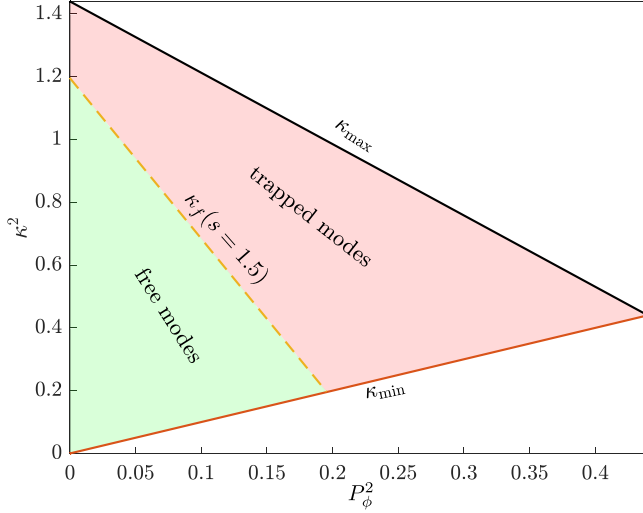


FIG. 4. Allowed range of κ as a function of P_ϕ for a prolate spheroid of aspect ratio 1.81, ($\xi = 1.2$). κ must lie in the shaded regions.

done by substituting κ_f into Eq. (29), and rearranging for $P_{\phi,f} = P_\phi(\kappa = \kappa_f)$ gives

$$P_{\phi,f} = \frac{\sin \varphi}{s} \sqrt{\frac{(1 - \eta^2)(\xi^2 - 1)[\xi^2 - 1 - (\eta^2 - 1)s^2]}{\xi^2 - 1 - (\eta^2 - 1)[s^2 - (s^2 - 1)\cos^2 \varphi]}}.$$

Now we can express p_f in terms of η and φ :

$$p_f = \frac{1}{s} \sqrt{\frac{\xi^2 - 1 + (1 - \eta^2)s^2}{\xi^2 - 1 + (1 - \eta^2)(s^2 - (s^2 - 1)\cos^2 \varphi)}}, \quad (31)$$

which satisfies $p_f \geq 1/s$ as required. $p_f(\varphi, t)$ is plotted in Fig. 5 for a representative spheroid, where t is the arc length

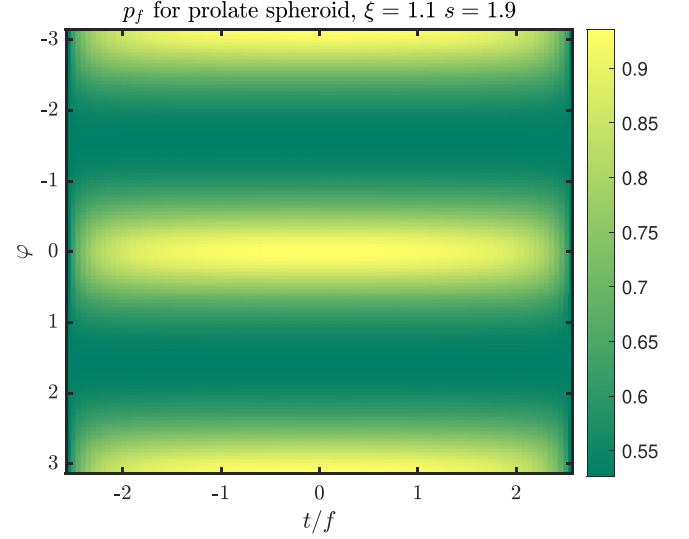


FIG. 5. Phase space p, φ, t for a prolate spheroid of aspect ratio 2.4, refractive index $s = 1.9$, where p is measured on the color scale. t is the arc length along a line of constant longitude and f is the half-focal length. The free modes lie below the surface $p = p_f(\varphi, t)$.

from the north pole. One may reparameterize p_f in terms of z through $\eta = z/c$, and we also have $\xi = c/f = c/\sqrt{c^2 - a^2}$.

C. Mean path length

With p_f we can now derive the mean path length under diffuse illumination. This is given by an integral over all free chords:

$$\langle L_{\text{pro}} \rangle = \frac{s^2}{\Sigma} \int_{-c}^c \int_0^{2\pi} \int_0^{\theta_f} C(\theta, \varphi, z) \rho \frac{dt}{dz} \sin 2\theta d\theta d\varphi dz, \quad (32)$$

where $\theta_f = \text{asin}(p_f)$, $\Sigma = 2\pi a^2(\xi \csc^{-1}(\xi)c/a + 1)$ is the surface area, $\rho = a\sqrt{1 - z^2/c^2}$ is the distance from the z axis, $\sin 2\theta$ is the angular distribution of diffuse rays incident on a surface in three dimensions, and the chord length C is derived in the Appendix to be

$$C = \frac{2a \cos \theta (a^2 z^2 - c^2 z^2 + c^4)^{3/2}}{a^2 c^2 z^2 \sin^2 \theta \sin^2 \varphi - c^4 \sin^2 \theta \cos^2 \varphi (c^2 - a^2 - z^2) - acz(c^2 - a^2)\sqrt{c^2 - z^2} \sin 2\theta \cos \varphi + a^4 z^2 \cos^2 \theta + c^4(c^2 - z^2)}. \quad (33)$$

Numerically the integral (32) agrees with Monte Carlo simulations to within their standard deviation of $\sim 10^{-4}$.

For a near spherical spheroid, the chord length (33) and the integral (32) can be expanded as a series about the eccentricity $e \rightarrow 0$:

$$\begin{aligned} \langle L_{\text{pro}} \rangle &= \frac{4c}{3s} (s^3 - (s^2 - 1)^{3/2}) \\ &\quad - \frac{2c}{9s} (2s^3 - 5(s^2 - 1)^{3/2})e^2 \\ &\quad - \frac{c}{270s} ((36s^2 - 41)(s^2 - 1)^{3/2} + 56s^3)e^4 + O(e^6), \end{aligned} \quad (34)$$

where the first term is the mean path length in a sphere. This expansion closely approximates the exact mean path length plotted in Fig. 7 for low aspect ratios.

We can now obtain the absorption of a weakly absorbing spheroid in the high-frequency limit. Both the absorption of a spheroid under diffuse illumination, and the orientation averaged absorption in a directional wave, are expressed as

$$C_{\text{abs}} = \frac{\Sigma}{4} \alpha \langle L \rangle, \quad (35)$$

where α is the absorption coefficient and $\Sigma/4$ is the orientation averaged surface area (due to Cauchy's theorem). The extinction cross section in this limit is twice the

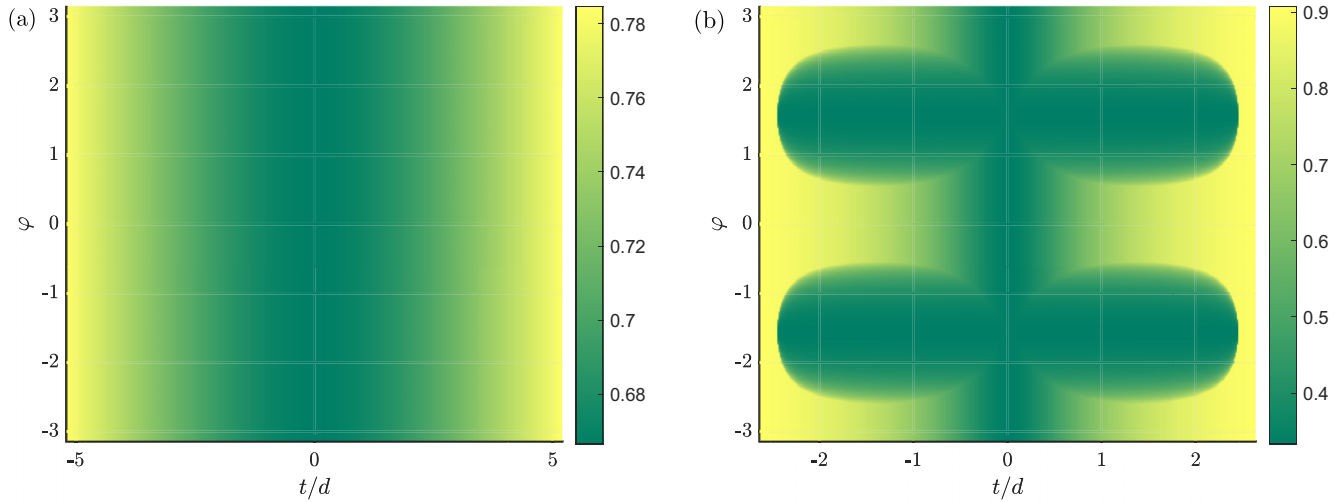


FIG. 6. Phase spaces for oblate spheroids of different aspect ratios and refractive indices, where p is measured on a color scale. (a) $c = 0.832a$ ($\chi = 1.5$) and $s = 1.5 < \sqrt{\chi^2 + 1}$. In this case $p_{f,\text{out}}$ is a smooth function of t and independent of φ , given by (36). (b) $c = 0.447a$ ($\chi = 0.5$) and $s = 3 > \sqrt{\chi^2 + 1}$. In this case the critical surface is the intersection of two curves, $p = \min(p_{f,\text{out}}, p_{f,\text{in}})$, where $p_{f,\text{out}}$ is given in Eq. (36) and $p_{f,\text{in}}$ in Eq. (39). t is the arc length from the equator and d is the focal disk radius.

cross-sectional area, i.e., $\Sigma/2$. Edge effect corrections may be added to account for first-order wave effects, but are not currently refractive index dependent for absorption [27–29].

IV. OBLATE SPHEROID

The derivations for the oblate spheroid are more complex than for the prolate spheroid, so the details are left for the Appendix. The mean path length is still obtained via integrating the chord lengths over the free phase space, except that for high aspect ratios, the boundary between the free and trapped phase space may be defined by the intersection of two surfaces. This is due to two different types of trajectory, inner modes that pass through the focal disk, and outer modes that do not.

We may define the surface by $\frac{\rho^2}{a^2} + \frac{z^2}{c^2} = 1$. The coordinate χ (analogous to ξ) also defines a surface, by fixing $\chi = c/d$ where $d = \sqrt{a^2 - c^2}$ is the focal disk radius. The angular coordinate is $\eta = z/c$ on the surface.

For $s \leq \sqrt{\chi^2 + 1}$, i.e., relatively low aspect ratio and refractive index, the outer modes are the only ones that can be trapped, and a single surface $p = p_{f,\text{out}}$ marks the boundary between the free and trapped modes:

$$p_{f,\text{out}} = \frac{1}{s} \sqrt{\frac{\chi^2 + \eta^2 s^2}{\chi^2 + \eta^2}}, \quad (36)$$

which is plotted in Fig. 6(a) for a representative spheroid. Note that it is independent of the angle φ .

The mean path length is then calculated as the following integral, expressed in z, φ, θ coordinates:

$$\langle L_{\text{obl}} \rangle = \frac{s^2}{\Sigma} \int_{-c}^c \int_0^{2\pi} \int_0^{\theta_{f,\text{out}}} C(\theta, \varphi, z) \rho \frac{dt}{dz} \sin 2\theta d\theta d\varphi dz, \quad (37)$$

where $\Sigma = 2\pi a^2 (\chi \text{csch}^{-1}(\chi) c/a + 1)$ is the surface area, $\theta_{f,\text{out}} = \text{asin}(p_{f,\text{out}})$, $\rho = a\sqrt{1 - z^2/c^2}$, and the chord length C is given in Eq. (33).

For a near spherical spheroid, the integral (37) and the chord length (33) can be expanded as a series of the (imaginary) parameter $e = c/\sqrt{c^2 - a^2}$:

$$\begin{aligned} \langle L_{\text{obl}} \rangle &= \frac{4c}{3s} (s^3 - (s^2 - 1)^{3/2}) \\ &\quad - \frac{2c}{9s} (2s^3 + (s^2 - 1)^{3/2}) e^2 \\ &\quad - \frac{c}{270s} (56s^3 + 19(s^2 - 1)^{3/2}) e^4 + O(e^6), \end{aligned} \quad (38)$$

which closely matches the exact mean path length for low aspect ratios as shown in Fig. 7. Note that the mean path length does not vary smoothly from prolate to oblate spheroids—the gradient changes at $e = 0$ ($h = 1$).

For $s \geq \sqrt{\chi^2 + 1}$, i.e., relatively high aspect ratio and refractive index, the trapped phase space also includes inner modes. The surface $p_{f,\text{in}}$ that divides the free and trapped modes of the inner type is given by

$$p_{f,\text{in}} = \frac{1}{s} \sqrt{\frac{(\eta^2 - 1)s^2 + \chi^2 + 1}{\chi^2 + 1 + (\eta^2 - 1)(s^2 - (s^2 - 1) \cos \varphi^2)}}. \quad (39)$$

The surfaces $p_{f,\text{in}}, p_{f,\text{out}}$ intersect at $\varphi = \varphi_{i/o}$ given by

$$\cos \varphi_{i/o} = \eta \sqrt{\frac{(\eta^2 - 1)s^2 + \chi^2 + 1}{(\eta^2 - 1)(\eta^2 s^2 + \chi^2)}}, \quad (40)$$

where $p_{f,\text{in}} < p_{f,\text{out}}$ for $\varphi > \varphi_{i/o}$ (due to the fourfold symmetry about φ we can focus on $0 \leq \varphi < \pi/2$). The combination

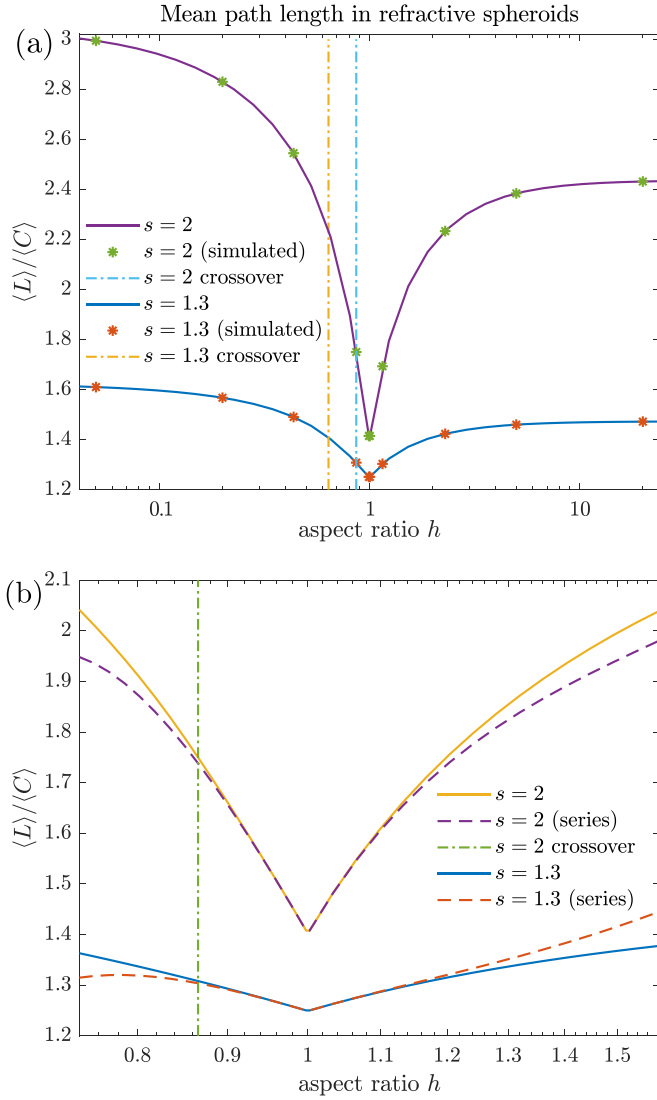


FIG. 7. (a) Mean path length in spheroids of varying aspect ratio h , normalized by the corresponding mean chord length. The stars are data from Monte Carlo simulations. In the scattering case the normalized mean path length would simply be s^2 , independent of h . For $h < 1$ the spheroid is oblate, and the dot-dash lines mark $s = \sqrt{\chi^2 + 1}$ (equivalently $h = \sqrt{1 - s^{-2}}$), where Eq. (41) is used to the left of the vertical dashed line and Eq. (37) is used to the right until $h = 1$. For $h > 1$, the prolate case, Eq. (32) is used. (b) Zoomed region near $h = 1$, showing the approximations (38) for $h \lesssim 1$ and (34) for $h \gtrsim 1$.

of the surfaces (36) and (39) is shown in Fig. 6(b). The mean path length is calculated as the piecewise integral [$\theta_{f,\text{in}} = \text{asin}(p_{f,\text{in}})$]:

$$\langle L_{\text{obl}} \rangle = \frac{4s^2}{\Sigma} \int_{-c}^c \left[\int_0^{\varphi_{i/o}} \int_0^{\theta_{f,\text{out}}} + \int_{\varphi_{i/o}}^{\pi/2} \int_0^{\theta_{f,\text{in}}} \right] \times C(\theta, \varphi, z) \rho(z) \frac{dt}{dz} \sin 2\theta d\theta d\varphi dz, \quad (41)$$

which numerically agrees with Monte Carlo simulations of 10^8 rays.

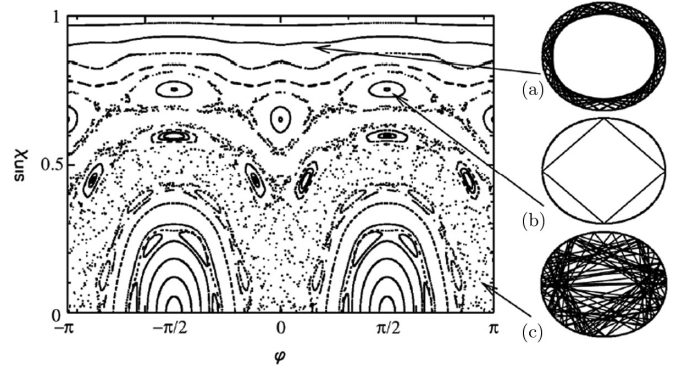


FIG. 8. Phase portrait of a quadrupole billiard, reprinted with permission from Ref. [16] ©The Optical Society, showing phase space curves and their respective orbits in the quadrupole (right). Half the phase space is shown, and $\sin \chi$ on the vertical axis is our p , and φ is the polar angle which is related to the arc length t .

Figure 7 plots the mean path length normalized by the mean chord length, with varying aspect ratio $h = c/a$, covering prolate and oblate spheroids using Eqs. (32), (37), (41) piecewise. The integrals for the oblate spheroids transition into each other smoothly. The mean path length is minimum for a sphere, which is related to the fact that a smaller range of orbits are accessible from outside in a sphere for a given refractive index: the phase space for a sphere is flat and the integration domain is simply $\theta < \theta_c$, whereas for spheroids the integration domain expands to include chords that can be reached via total internal reflection.

V. ERGODICITY, BILLIARD THEORY, AND MEAN PATH LENGTH

Let us discuss the implications of this proposed approach on the mean path length for a general shape. We have seen that ellipses are nonergodic, which means that any given ray maps out a fixed curve in the phase space. Some of these curves are trapped from the perspective of refraction through the boundary. Only a specific few shapes are completely nonergodic, while most shapes will at least contain ergodic regions in their phase space, where the dynamics are chaotic but confined to these subregions. Examples of this are Limaçons [13,15,35,36] and tunable circular-polygonal billiards [37]. Any convex shape with a sufficiently smooth boundary has a nonergodic region near $p \rightarrow \pm 1$, where the orbits are whispering gallery modes [38]. These modes also have very short chords so their absence only subtracts a tiny amount from the mean path length, that is, $\langle L \rangle \lesssim \langle L_{\text{sca}} \rangle$. A representative example of a partially ergodic phase space is shown in Fig. 8 for a quadrupole (squashed circle) billiard. The dotted ergodic regions surround islands of stability and at the top are the whispering gallery modes. To calculate $\langle L \rangle$ using Eq. (12), we would make $p_f(t)$ the lowest curve such that all curves and ergodic regions above $p_f(t)$ do not bleed into the region $p < 1/s$. Unfortunately, analytic expressions for curves in the phase portraits of most billiards are rare, so the integral would have numerical bounds.

In a fully ergodic (closed) billiard, every ray covers the whole phase space, so there are no trapped modes in the

open billiard. Therefore in Eq. (12) we set $p_f = 1$, which leads to $\langle L \rangle = \langle L_{\text{sca}} \rangle$ for all refractive indices. Of course in an experimental setting no refractive object has a perfectly analytical boundary, and we should expect that the boundary imperfections make the dynamics completely ergodic, so the mean path length in any case is simply $\langle L \rangle = \langle L_{\text{sca}} \rangle$. Then any idealized simulation or calculation of $\langle L \rangle$ such as the one conducted in this paper will be an underestimate of the physical value. Even adding infinitesimally small imperfections to the boundary of an idealized shape introduces orbits, which are confined to the (previously) trapped phase space for an arbitrarily long time, yet still accessible. Nevertheless, the idealized value for $\langle L \rangle$ should still provide the correct approximation to the absorption of a weak absorber. This was argued in Refs. [1,2] in the case of a small scattering coefficient and for a regular polygon with a very large number of sides, approaching a circle. The idea is that the arbitrarily long trajectories that are introduced by the small imperfections get absorbed early on anyway, and therefore have a negligible contribution to the mean path length because of their scarcity. This scenario relies on the rate of absorption being significantly higher than the rate of diffusion due to the imperfections, but also that the absorption be not too high as to significantly affect the typical paths of rays that behave as they would in the idealized case. Whether this scenario occurs in nature or is feasible to create in a laboratory is another question.

VI. CONCLUSION

This paper demonstrates the link between billiard theory and optical mean path length, where the concept of the phase portrait provides an elegant alternative to brute force calculation of individual path lengths. The link has the immediate consequence for ergodic shapes that the mean path length is equal to that in the scattering case. This implies that in an imperfect experimental setting, the mean path length will always be equal to scattering mean path length. However, we have argued that the idealized value for the mean path length is relevant for calculating absorption in some limits.

Specifically we have derived analytic expressions for the mean path length in ellipses and spheroids, by integrating the chord length over the free regions of the phase space. For the ellipse we found the phase space curves corresponding to rays on the boundary between being free and trapped, for which we integrated the chord lengths below this curve. For spheroids the curves generalized to surfaces in a 3D phase space, determined by two constants of motion. We examined the relationship between the parameter space of constants of motion and the phase space, and found that the two types of orbit in the oblate spheroid create a two piece boundary between free and trapped modes. Our analytic expressions for the mean path length may be applied to calculating the absorption of large weakly absorbing spheroids, and the series expansions for small eccentricity provide fast approximations for modeling near-spherical particles.

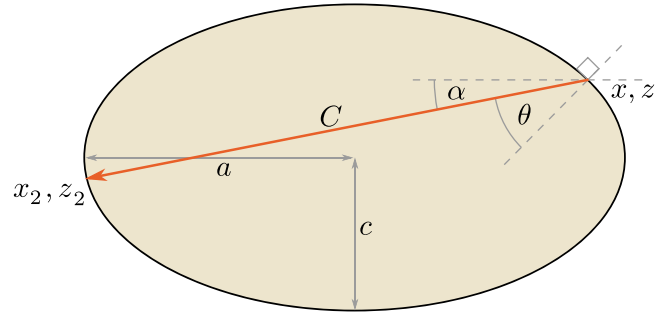


FIG. 9. Chord in an ellipse.

ACKNOWLEDGMENTS

The authors are grateful to The MacDiarmid Institute New Zealand and a Whitinga fellowship for financial support.

APPENDIX A: CHORD LENGTH IN AN ELLIPSE

Here we calculate the chord length of a ray that enters the ellipse at a point $x \geq 0, z \geq 0$ on the boundary (where $x = a\sqrt{1 - z^2/c^2}$), with an angle θ to the normal as shown in Fig. 9. The chord length C is the distance from (x, z) to the next point that the ray hits the boundary at x_2, z_2 . This may be expressed as

$$C = \frac{z - z_2}{\sin \alpha}, \quad (\text{A1})$$

where α is the angle between the ray and the x axis, which is related to θ by

$$\alpha = \text{atan}(m_n) + \theta \quad (\text{A2})$$

and

$$m_n = \frac{az}{c\sqrt{c^2 - z^2}} \quad (\text{A3})$$

is the gradient of the normal at point x, z . The equation of a straight line $(z - z_2) = (x - x_2) \tan \alpha$ gives z_2 as

$$z_2 = \frac{c^2 z - a^2 \tan^2 \alpha z - 2ac\sqrt{c^2 - z^2} \tan \alpha}{c^2 + a^2 \tan^2 \alpha}. \quad (\text{A4})$$

Then combining Eq. (A1) with (A4) and (A2), and using the sum angle formulas gives the chord length (6).

APPENDIX B: CHORD LENGTH IN A SPHEROID

Here we calculate the chord length of a ray that enters at x, y, z with angle θ to the normal, φ around the normal, where $\varphi = 0$ points towards the north pole of the spheroid. This derivation applies for both prolate and oblate spheroids. Without loss of generality we may let the incident ray hit $x \geq 0$ and $y = 0$. We can project the problem on to the xz plane and follow the derivation for the ellipse, but this time what was the chord length becomes the major axis of an elliptic cross section \bar{E} whose major axis subtends an angle θ' from the surface normal and whose minor axis is parallel to the y axis, as depicted in Fig. 10. The ray lies on this ellipse and its trajectory is defined by a second angle ϕ' which varies

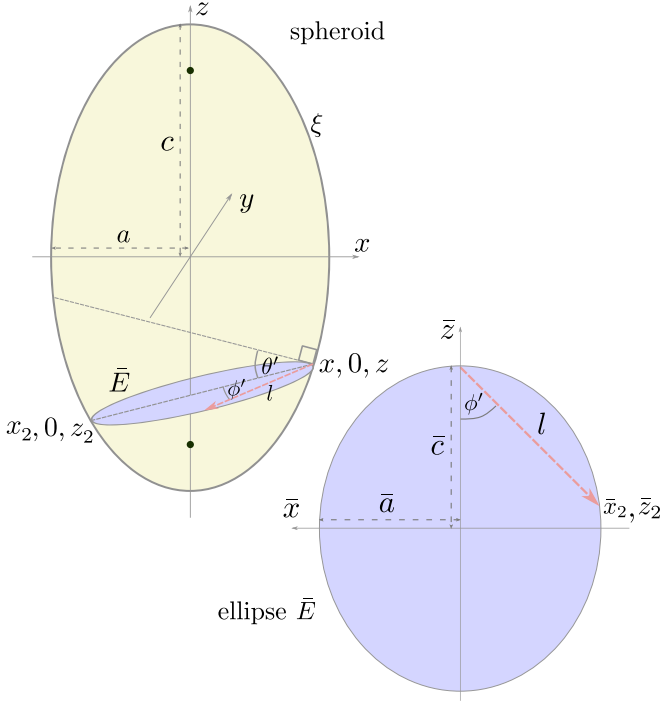


FIG. 10. Schematic of a ray (thick dashed arrow) across a spheroid, and flat view of the ray lying on the elliptic section \bar{E} .

perpendicular to θ' . The angles θ' and ϕ' can be related to the angles θ , ϕ by inspection of Fig. 11:

$$\tan \theta' = \tan \theta \cos \phi \quad (\text{B1})$$

$$\sin \phi' = \sin \theta \sin \phi. \quad (\text{B2})$$

Looking at the spheroid, the gradient of the ray in the θ' direction (the gradient of the projection of the ray onto the

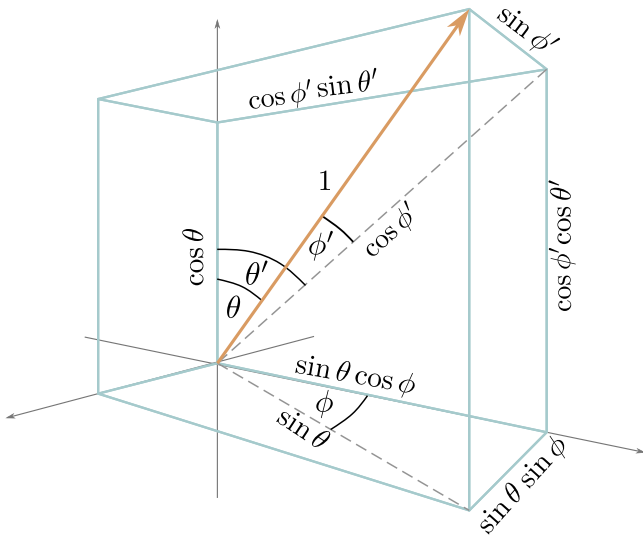


FIG. 11. Decomposition of the angles θ , ϕ into components θ' , ϕ' . The light ray (bold solid arrow) enters the particle from below and travels a unit distance into the spheroid. The cube is not real and only to visualize the angles more clearly.

$y = 0$ plane) is

$$m_\theta = \tan(\text{atan}(m_n) + \theta'), \quad (\text{B3})$$

where $m_n = \frac{az}{c\sqrt{c^2-z^2}}$ is the gradient of the normal at the incident point. We denote $x_2, y_2 = 0, z_2$ as the 3D coordinates of the opposite end of the ellipse arE . x_2 and z_2 may be calculated as

$$z_2 = \frac{c^2 z - a^2 m_\theta^2 z - 2acm_\theta \sqrt{c^2 - z^2}}{c^2 + a^2 m_\theta^2}$$

$$x_2 = x - \frac{z - z_2}{m_\theta}. \quad (\text{B4})$$

On the ellipse \bar{E} , we denote the semimajor and semiminor axes by \bar{c} and \bar{a} , the Cartesian coordinates by \bar{x}, \bar{z} , and the ray's exit point by \bar{x}_2, \bar{z}_2 , as shown in Fig. 10. \bar{c} is found from the half-distance from x, z to x_2, z_2 :

$$\bar{c} = \frac{1}{2} \sqrt{(x - x_2)^2 + (z - z_2)^2} \quad (\text{B5})$$

and \bar{a} can be obtained from the intersection of the spheroid surface at $(\frac{x+x_2}{2}, y = \bar{a}, \frac{z+z_2}{2})$:

$$\bar{a} = a \sqrt{1 - \left(\frac{z+z_2}{2c}\right)^2 - \left(\frac{x+x_2}{2a}\right)^2}. \quad (\text{B6})$$

The chord length C is the distance across this ellipse from the tip $\bar{x} = 0, \bar{z} = \bar{c}$ to the exit point \bar{x}_2, \bar{z}_2 :

$$C = \frac{\bar{c} - \bar{z}_2}{\cos \phi'}. \quad (\text{B7})$$

ϕ' is defined in Eq. (B2), and \bar{z}_2 is found by solving $\bar{z}_2 - \bar{c} = m_\phi \bar{x}_2$, where $m_\phi = -\cot \phi'$ is the gradient of the ray in \bar{E} :

$$\bar{z}_2 = \frac{2\bar{c}^3}{\bar{c}^2 + \bar{a}^2 m_\phi^2} - \bar{c}. \quad (\text{B8})$$

Substituting \bar{z}_2, \bar{c} and ϕ' in to Eq. (B7) gives the chord length (33) for both prolate and oblate spheroids.

APPENDIX C: MEAN PATH LENGTH IN AN OBLATE SPHEROID

Here we cover the details in deriving the mean path length for the oblate spheroid. The oblate spheroidal coordinates are

$$\chi = i \frac{\sqrt{(z+f)^2 + \rho^2} + \sqrt{(z-f)^2 + \rho^2}}{2f} \quad (\text{C1})$$

$$\eta = \frac{\sqrt{(z+f)^2 + \rho^2} - \sqrt{(z-f)^2 + \rho^2}}{2f}, \quad (\text{C2})$$

where $f = \sqrt{c^2 - a^2}$ is imaginary, a is the half width, c the half-height, and the focal disk radius is $d = -if$. χ is real and defines the surface by $\chi = c/d$.

1. Constants of motion

The oblate constants of motion are not just a reparameterization of those the prolate spheroid; there are a few surprising differences, which alter the analysis significantly. So we will outline the derivation of Ref. [33] to determine the constants of motion.

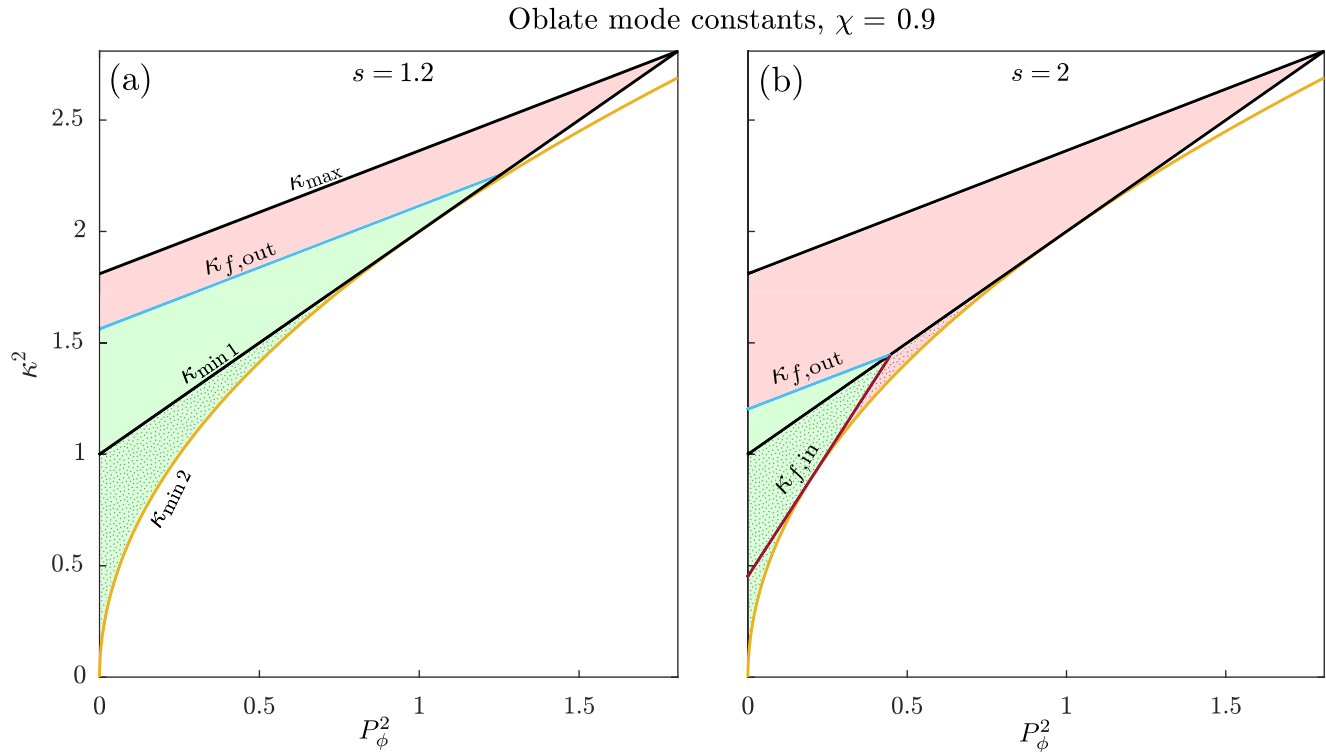


FIG. 12. Allowed range of κ as a function of P_ϕ : κ must lie in the colored regions. The red (top) region corresponds to trapped modes, green (bottom) to free modes, and the dotted to inner modes. For $s = 1.2$, which is less than $\sqrt{\chi^2 + 1}$, the line $\kappa_{f,\text{out}}$ lies entirely in the outer mode region and defines the boundary of free modes without the need for $\kappa_{f,\text{in}}$. For $s = 2 > \sqrt{\chi^2 + 1}$, $\kappa_{f,\text{out}}$ intersects $\kappa_{f,\text{in}}$ at the boundary of inner and outer modes, at \hat{p}_ϕ . For $\kappa < \kappa_{\text{min}1}$, $\kappa_{f,\text{in}}$ defines the maximal free modes above the intersection $\kappa_{f,\text{in}} = \kappa_{\text{min}2}$.

The Hamiltonian in oblate spheroidal coordinates is expressed in terms of the conjugate momenta as

$$H = \frac{1}{2} \left(\frac{\chi^2 + 1}{\chi^2 + \eta^2} P_\chi^2 + \frac{1 - \eta^2}{\chi^2 + \eta^2} P_\eta^2 + \frac{P_\phi^2}{(\chi^2 + 1)(1 - \eta^2)} \right). \quad (\text{C3})$$

Fixing $H = 1/2$, this may be separated by multiplying by $\chi^2 + \eta^2$, rearranging into χ and η dependent sides and setting both sides equal to a positive constant κ^2 :

$$(1 + \chi^2)(1 - P_\chi^2) + \frac{P_\phi^2}{1 + \chi^2} = \kappa^2 \quad (\text{C4})$$

$$(1 - \eta^2)(1 + P_\eta^2) + \frac{P_\phi^2}{1 - \eta^2} = \kappa^2. \quad (\text{C5})$$

We added 1 to each equation so that κ is proportional to the definition in Ref. [33], where κ reduces to the angular momentum in the spherical case. The other constant of motion is again P_ϕ . Following the same approach as for the prolate spheroid, we can show that P_ϕ lies in the range

$$0 \leq P_\phi^2 \leq \chi^2 + 1. \quad (\text{C6})$$

The range of κ is not as simple as for the prolate spheroid. Its maximum occurs for rays grazing the surface with $P_\chi = 0$; here Eq. (C4) gives

$$\kappa_{\text{max}}^2 = 1 + \chi^2 + \frac{P_\phi^2}{1 + \chi^2}. \quad (\text{C7})$$

κ_{min} depends casewise on P_ϕ , and can be found by analyzing Eq. (C5) with $P_\eta = 0$. If $P_\phi^2 > 1$, the minimum occurs at $\eta = 0$, where $\kappa^2 = P_\phi^2 + 1$ and the ray travels in the xy plane outside the focal disk. If $P_\phi^2 < 1$, then minima lie at $\eta^2 = 1 - |P_\phi|$, where $\kappa^2 = 2|P_\phi|$, and the ray crosses the focal disk, in and out of the xy plane. In summary,

$$\kappa_{\text{min}}^2 = \begin{cases} \kappa_{\text{min}1}^2 = P_\phi^2 + 1 & P_\phi^2 < 1 \\ \kappa_{\text{min}2}^2 = 2|P_\phi| & P_\phi^2 \geq 1 \end{cases}. \quad (\text{C8})$$

The allowed range of values of κ , P_ϕ is plotted in Fig. 12. Reference [33] discusses two types of modes and their conditions in terms of P_ϕ and κ . Type 1, which we will call outer modes, do not cross the focal disk and tend to circle around the spheroid. Type 2 or inner modes pass through the focal disk.¹

The domain of inner modes is the region $\kappa_{\text{min}2} \leq \kappa \leq \kappa_{\text{min}1}$ (dotted region in Fig. 12), over the interval $P_\phi^2 \leq 1$. There are no inner modes for $P_\phi^2 > 1$ because the minimum approach of rays to the rotation axis is greater than the focal disk radius.

¹In fact a similar distinction could have been made for prolate spheroids depending on whether the rays pass through the focal segment, but only a vanishing quantity of rays pass exactly through the focal segment, so for the purposes of calculating mean path length we could treat all modes as being outer.

2. Phase space and the boundary between free and trapped modes

Now we would like to obtain the phase space curves $p(\eta, \kappa, P_\phi)$, $\varphi(\eta, \kappa, P_\phi)$. For the oblate spheroid $p = \sin \theta$ may be calculated as

$$p = \frac{\sqrt{v_\eta^2 + v_\phi^2}}{\sqrt{v_\chi^2 + v_\eta^2 + v_\phi^2}}, \quad (\text{C9})$$

where the velocities can be converted into conjugate momenta via

$$v_\chi = \sqrt{\frac{\chi^2 + 1}{\chi^2 + \eta^2}} P_\chi \quad (\text{C10})$$

$$v_\eta = \sqrt{\frac{1 - \eta^2}{\chi^2 + \eta^2}} P_\eta \quad (\text{C11})$$

$$v_\phi = \frac{P_\phi}{\sqrt{(\chi^2 + 1)(1 - \eta^2)}} \quad (\text{C12})$$

and P_χ, P_η can be expressed in terms of κ, P_ϕ , and η by solving Eqs. (C4), (C5):

$$P_\chi = \sqrt{\frac{-\kappa^2}{\chi^2 + 1} + \frac{P_\phi^2}{(\chi^2 + 1)^2} + 1} \quad (\text{C13})$$

$$P_\eta = \sqrt{\frac{\kappa^2}{1 - \eta^2} - \frac{P_\phi^2}{(1 - \eta^2)^2} - 1}. \quad (\text{C14})$$

P_χ is always real, while P_η is only real for a range of $\eta_{0-} \leq |\eta| \leq \eta_{0+}$ where

$$\eta_{0\pm} = \sqrt{1 - \frac{\kappa^2}{2} \pm \sqrt{\frac{\kappa^4}{4} - P_\phi^2}}. \quad (\text{C15})$$

This will affect the boundary between free and trapped modes for high s , in Sec. C.

Any pair of constants κ, P_ϕ defines a curve $p(\eta), \varphi(\eta)$ on the phase space. Such a curve $p(\eta)$ can be expressed in terms of η, κ, P_ϕ by using Eqs. (C9)–(C14) as

$$p(\eta, \kappa, P_\phi) = \sqrt{\frac{\kappa^2 - 1 - P_\phi^2 + \eta^2 + (\kappa^2 - 1 + \eta^2)\chi^2}{(1 + \chi^2)(\eta^2 + \chi^2)}} \quad (\text{C16})$$

and for $\varphi(\eta, \kappa, P_\phi)$,

$$\begin{aligned} \cos \varphi &= \frac{v_\eta}{\sqrt{v_\eta^2 + v_\phi^2}} \\ &= \pm \sqrt{\frac{1 + \chi^2 \kappa^2 - P_\phi^2 - 1 + \eta^2 - \eta^2(\kappa^2 - 1 + \eta^2)}{1 - \eta^2 \kappa^2 - P_\phi^2 - 1 + \eta^2 + \chi^2(\kappa^2 - 1 + \eta^2)}}. \end{aligned} \quad (\text{C17})$$

To express a phase space surface $p(\eta, \varphi)$, we must define some function $\kappa(P_\phi)$ as we did for the prolate spheroid.

The integration domain over free chords is the volume bounded between surfaces $p = 0$ and $p_f(\eta, \varphi)$, which is the lowest surface such that $p_f \geq 1/s$ everywhere. Again in order to find p_f , we must find where p is minimized in terms of η ,

and equate this to $1/s$ to find the critical curve $\kappa_f(P_\phi)$. To do this we will need to break down case by case depending on s .

3. Case $s \leq \sqrt{\chi^2 + 1}$

This is the simpler case where all inner modes are free. The inner mode region illustrated in the κ, P_ϕ space in Fig. 12 where the inner modes lie in the region $\kappa_{\min 2} \leq \kappa \leq \kappa_{\min 1}$. For $s \leq \sqrt{\chi^2 + 1}$ the boundary between the trapped and free phase spaces is defined by a surface of outer orbits. For outer orbits p is minimum at $\eta = 0$, and the condition $p(\eta = 0, P_\phi, \kappa = \kappa_{f,\text{out}}(P_\phi)) = 1/s$ tells us the critical curve $\kappa_{f,\text{out}}(P_\phi)$:

$$\kappa_{f,\text{out}} = \sqrt{1 + \frac{\chi^2}{s^2} + \frac{P_\phi^2}{\chi^2 + 1}}. \quad (\text{C18})$$

The boundary is simply determined by $\kappa \leq \kappa_{f,\text{out}}$, and this gives for $p_{f,\text{out}} = p(\eta, P_\phi, \kappa = \kappa_{f,\text{out}})$ (note that the P_ϕ dependence drops out unlike for the prolate case):

$$p_{f,\text{out}} = \frac{1}{s} \sqrt{\frac{\chi^2 + \eta^2 s^2}{\chi^2 + \eta^2}}, \quad (\text{C19})$$

which is Eq. (36) in the main text, and the mean path length may then be calculated from the integral (37).

4. Case $s > \sqrt{\chi^2 + 1}$

For $s > \sqrt{\chi^2 + 1}$ not all inner orbits are free. Rays in inner orbits may not reach $\eta = 0$, so p is minimum at $\eta = \pm \eta_{0\pm}$. The condition $p(\eta_{0\pm}, P_\phi, \kappa_{f,\text{in}}) = 1/s$ [conveniently $p(\eta_{0+}, P_\phi, \kappa) = p(\eta_{0-}, P_\phi, \kappa)$] tells us the critical curve $\kappa_{f,\text{in}}(P_\phi)$:

$$\kappa_{f,\text{in}}^2 = \frac{\chi^2 + 1}{s^2} + \frac{s^2 P_\phi^2}{\chi^2 + 1}. \quad (\text{C20})$$

$\kappa_{f,\text{in}}$ is only relevant in the range of inner orbits, $\kappa < \kappa_{\min 1}$, and is plotted in Fig. 12(b) for a representative spheroid.

The corresponding surface $p_{f,\text{in}}$ may be expressed in terms of η, φ as

$$p_{f,\text{in}} = \frac{1}{s} \sqrt{\frac{(\eta^2 - 1)s^2 + \chi^2 + 1}{\chi^2 + 1 + (\eta^2 - 1)(s^2 - (s^2 - 1)\cos^2 \varphi)}}, \quad (\text{C21})$$

which is Eq. (39) of the main text.

Now we have two surfaces $p_{f,\text{in}}$ and $p_{f,\text{out}}$, which define the boundary between free and trapped modes. $p_{f,\text{out}} \leq p_{f,\text{in}}$ occurs only for $s \geq \sqrt{\frac{\chi^2 + 1}{1 - \eta^2}}$, or more generally if $s \geq \sqrt{\chi^2 + 1}$. So for $s \leq \sqrt{\chi^2 + 1}$, the domain of free modes is simply $p \leq p_{f,\text{out}}$, while for $s > \sqrt{\chi^2 + 1}$ we have to consider the intersection of $p_{f,\text{out}}$ and $p_{f,\text{in}}$.

The expression (C21) is of an analogous form to Eq. (31) in the prolate case but here it actually contains three

disjoint surfaces on either sides of $\eta_i = \pm\sqrt{s^2 - \chi^2 - 1}/s$. For $|\eta| > \eta_i$, Eq. (C21) has real values, which correspond to inner modes, which are all free, analogous to the inner modes in an ellipse. In Fig. 12(b) these lie on the line segment $\kappa_{f,\text{in}}$ left of the intersection with $\kappa_{\text{min}2}$, but these do not represent the boundary between free and trapped modes. So for $|\eta| > \eta_i$, the boundary for free modes is simply $p_{f,\text{out}}$. For $|\eta| \leq \eta_i$, the surfaces $p_{f,\text{in}}$ and $p_{f,\text{out}}$ intersect, so we integrate from $p = 0$

to $\min(p_{f,\text{in}}, p_{f,\text{out}})$ over this interval. The surfaces intersect at $\varphi = \varphi_{i/o}$ given by

$$\cos \varphi_{i/o} = \eta \sqrt{\frac{(\eta^2 - 1)s^2 + \chi^2 + 1}{(\eta^2 - 1)(\eta^2 s^2 + \chi^2)}}, \quad |\eta| \leq |\eta_i|, \quad (\text{C22})$$

which is Eq. (40) of the main text. To obtain the mean path length we integrate to $p_{f,\text{in}}$ over the interval $\varphi > \varphi_{i/o}$, and integrate to $p_{f,\text{out}}$ otherwise, giving Eq. (41).

-
- [1] M. Majic, W. R. C. Somerville, and E. C. Le Ru, Mean path length inside nonscattering refractive objects, *Phys. Rev. A* **103**, L031502 (2021).
- [2] M. Majic and W. R. C. Somerville, Mean path length in refractive regular polygons and prisms, *Phys. Rev. A* **105**, 023518 (2022).
- [3] T. Wriedt, A review of elastic light scattering theories, *Part. Part. Syst. Charact.: Measurement and Description of Particle Properties and Behavior in Powders and Other Disperse Systems* **15**, 67 (1998).
- [4] E. Czuber, Zur theorie der geometrischen wahrscheinlichkeiten, *Sitzungsber. Akad. Wiss. Wien* **90**, 719 (1884).
- [5] A. M. Kellerer, Considerations on the random traversal of convex bodies and solutions for general cylinders, *Radiat. Res.* **47**, 359 (1971).
- [6] R. Coleman, Random paths through convex bodies, *J. Appl. Probab.* **6**, 430 (1969).
- [7] W. J. M. De Kruijf and J. L. Kloosterman, On the average chord length in reactor physics, *Ann. Nucl. Energy* **30**, 549 (2003).
- [8] S. Blanco and R. Fournier, An invariance property of diffusive random walks, *Europhys. Lett.* **61**, 168 (2003).
- [9] R. Savo, R. Pierrat, U. Najar, R. Carminati, S. Rotter, and S. Gigan, Observation of mean path length invariance in light-scattering media, *Science* **358**, 765 (2017).
- [10] F. Martelli, F. Tommasi, L. Fini, L. Cortese, A. Sassaroli, and S. Cavalieri, Invariance properties of exact solutions of the radiative transfer equation, *J. Quant. Spectrosc. Radiat. Transfer* **276**, 107887 (2021).
- [11] I. Braun, G. Ihlein, F. Laeri, J. U. Nöckel, G. Schulz-Ekloff, F. Schüth, U. Vietze, Ö. Weiß, and D. Wöhrle, Hexagonal microlasers based on organic dyes in nanoporous crystals, *Appl. Phys. B: Lasers Opt.* **70**, 335 (2000).
- [12] J. Wiersig, Hexagonal dielectric resonators and microcrystal lasers, *Phys. Rev. A* **67**, 023807 (2003).
- [13] J.-B. Shim, A. Eberspächer, and J. Wiersig, Adiabatic formation of high-q modes by suppression of chaotic diffusion in deformed microdiscs, *New J. Phys.* **15**, 113058 (2013).
- [14] M. Kraft and J. Wiersig, Perturbative analysis of whispering-gallery modes in limaçon-shaped microcavities, *Phys. Rev. A* **89**, 023819 (2014).
- [15] H. Cao and J. Wiersig, Dielectric microcavities: Model systems for wave chaos and non-hermitian physics, *Rev. Mod. Phys.* **87**, 61 (2015).
- [16] H. E. Tureci, H. Schwefel, A. D. Stone, and E. Narimanov, Gaussian-optical approach to stable periodic orbit resonances of partially chaotic dielectric micro-cavities, *Opt. Express* **10**, 752 (2002).
- [17] S. Shinohara, T. Harayama, T. Fukushima, M. Hentschel, T. Sasaki, and E. E. Narimanov, Chaos-Assisted Directional Light Emission from Microcavity Lasers, *Phys. Rev. Lett.* **104**, 163902 (2010).
- [18] E. G. Altmann, J. S. E. Portela, and T. Tél, Leaking chaotic systems, *Rev. Mod. Phys.* **85**, 869 (2013).
- [19] D. J. Wilaard, M. I. Mishchenko, A. Macke, and B. E. Carlson, Improved T-matrix computations for large, nonabsorbing and weakly absorbing nonspherical particles and comparison with geometrical-optics approximation, *Appl. Opt.* **36**, 4305 (1997).
- [20] L. Bi and P. Yang, Physical-geometric optics hybrid methods for computing the scattering and absorption properties of ice crystals and dust aerosols, in *Light Scattering Reviews 8* (Springer, Berlin, 2013), pp. 69–114
- [21] L.-H. Sun, L. Bi, and B. Yi, The use of superspheroids as surrogates for modeling electromagnetic wave scattering by ice crystals, *Remote Sensing* **13**, 1733 (2021).
- [22] K. Muinonen, Scattering of light by crystals: a modified kirchhoff approximation, *Appl. Opt.* **28**, 3044 (1989).
- [23] A. Macke, Scattering of light by polyhedral ice crystals, *Appl. Opt.* **32**, 2780 (1993).
- [24] A. Macke, J. Mueller, and E. Raschke, Single scattering properties of atmospheric ice crystals, *J. Atmos. Sci.* **53**, 2813 (1996).
- [25] P. Yang and K. Liou, Light scattering by hexagonal ice crystals: solutions by a ray-by-ray integration algorithm, *J. Opt. Soc. Am. A* **14**, 2278 (1997).
- [26] B. Sun, P. Yang, G. W. Kattawar, and X. Zhang, Physical-geometric optics method for large size faceted particles, *Opt. Express* **25**, 24044 (2017).
- [27] L. Bi, P. Yang, G. W. Kattawar, and R. Kahn, Single-scattering properties of triaxial ellipsoidal particles for a size parameter range from the rayleigh to geometric-optics regimes, *Appl. Opt.* **48**, 114 (2009).
- [28] L. Bi and P. Yang, High-frequency extinction efficiencies of spheroids: Rigorous t-matrix solutions and semi-empirical approximations, *Opt. Express* **22**, 10270 (2014).
- [29] N. Okeudo, J. Ding, P. Yang, and R. Saravanan, Edge effect correction formula for superspheroids using the debye series, *Opt. Express* **30**, 146 (2022).
- [30] E. Yablouovitch, Statistical ray optics, *J. Opt. Soc. Am.* **72**, 899 (1982).
- [31] M. V. Berry, Regularity and chaos in classical mechanics, illustrated by three deformations of a circular 'billiard', *Eur. J. Phys.* **2**, 91 (1981).
- [32] F. Lenz, F. K. Diakonov, and P. Schmelcher, Scattering dynamics of driven closed billiards, *Europhys. Lett.* **79**, 20002 (2007).

- [33] P. H. Richter, A. Wittek, M. P. Kharlamov, and A. P. Kharlamov, Action integrals for ellipsoidal billiards, *Z. Naturforsch. A* **50**, 693 (1995).
- [34] H. Waalkens and H. R. Dullin, Quantum monodromy in prolate ellipsoidal billiards, *Ann. Phys. (NY)* **295**, 81 (2002).
- [35] H. R. Dullin and A. Bäcker, About ergodicity in the family of limaçon billiards, *Nonlinearity* **14**, 1673 (2001).
- [36] A. Bäcker and R. Schubert, Amplitude distribution of eigenfunctions in mixed systems, *J. Phys. A: Math. Gen.* **35**, 527 (2002).
- [37] D. R. da Costa, A. Fujita, M. R. Sales, J. D. Szezech Jr, and A. M. Batista, Dynamical properties for a tunable circular to polygonal billiard, *Braz. J. Phys.* **52** (2021).
- [38] V. F. Lazutkin, The existence of caustics for a billiard problem in a convex domain, *Math. USSR-Izvestiya* **7**, 185 (1973).